ORIGINAL ARTICLE

Spectral and Anatomical Patterns of Large-Scale Synchronization Predict Human Attentional Capacity

Santeri Rouhinen[1,2], Felix Siebenhühner[1], J. Matias Palva[1,3,4] and Satu Palva[1,3],

[1]Neuroscience Center Unit, Helsinki Institute of Life Science, University of Helsinki, Helsinki FI-00014, Finland, [2]BioMag Laboratory Unit, HUS Medical Imaging Center, Helsinki FI-00029, Finland, [3]Centre for Cognitive Neuroscience Unit, Institute of Neuroscience and Psychology, University of Glasgow, Glasgow G12 8Q8, UK and [4]Department of Neuroscience and Biomedical Engineering, Aalto University, Espoo FI-00076, Finland

Address correspondence to Santeri Rouhinen, Neuroscience Center, Helsinki Institute of Life Sciences, University of Helsinki, Haartmaninkatu 3, PO Box 21, FI-00014-University of Helsinki, Finland. Email: santeri.rouhinen@helsinki.fi; or Satu Palva, Email: satu.palva@helsinki.fi.

Abstract

The capacity of visual attention determines how many visual objects may be perceived at any moment. This capacity can be investigated with multiple object tracking (MOT) tasks, which have shown that it varies greatly between individuals. The neuronal mechanisms underlying capacity limits have remained poorly understood. Phase synchronization of cortical oscillations coordinates neuronal communication within the fronto-parietal attention network and between the visual regions during endogenous visual attention. We tested a hypothesis that attentional capacity is predicted by the strength of pretarget synchronization within attention-related cortical regions. We recorded cortical activity with magneto- and electroencephalography (M/EEG) while measuring attentional capacity with MOT tasks and identified large-scale synchronized networks from source-reconstructed M/EEG data. Individual attentional capacity was correlated with load-dependent strengthening of theta (3–8 Hz), alpha (8–10 Hz), and gamma-band (30–120 Hz) synchronization that connected the visual cortex with posterior parietal and prefrontal cortices. Individual memory capacity was also preceded by crossfrequency phase–phase and phase–amplitude coupling of alpha oscillation phase with beta and gamma oscillations. Our results show that good attentional capacity is preceded by efficient dynamic functional coupling and decoupling within brain regions and across frequencies, which may enable efficient communication and routing of information between sensory and attentional systems.

Key words: attention, capacity, EEG, MEG, oscillation, synchronization

Introduction

Studies using multiple-object tracking (MOT) tasks, where subjects attend and track one or more visual objects, have shown that humans have the capacity to concurrently attend to 2–4 moving visual objects (Pylyshyn and Storm 1988; Cowan 2001; Oksama and Hyona 2004; Treisman 2006; Bettencourt et al. 2011). The tracking of multiple objects among distractors is dependent on the selection of which items will be tracked (Lahnakoski et al. 2017) as well as on the sustained attention to the selected target objects (Alvarez and Cavanagh 2005). Interestingly, a similar capacity limit of 2–4 objects has also been observed for both visual working memory (VWM) (Luck and Vogel 1997; Cowan et al. 2005) and attention (Pylyshyn and Storm 1988; Treisman 2006; Bettencourt et al. 2011), so that VWM and attentional capacities are correlated in individual subjects (Oksama and Hyona 2004). These findings suggest that capacity limits of VWM and attention may stem from shared underlying neuronal mechanisms. Accordingly, the activation of

prefrontal (PFC), posterior-parietal (PPC), and visual cortices in functional magnetic resonance imaging (fMRI) data is characteristic to not only VWM tasks but also to MOT (Culham et al. 1998; Battelli et al. 2001; Jovicich et al. 2001; Howe et al. 2009; Alnaes et al. 2015), spatial attention (for reviews, see Kastner and Ungerleider 2000; Corbetta and Shulman 2002) and feature-based attention (Zhou and Desimone 2011), so that the connectivity within fronto-parietal attention networks mediate top–down attentional effects (Daitch et al. 2013; Spadone et al. 2015; Meehan et al. 2017). In the fronto-parietal system, PPC is one of the key regions where VWM capacity limits may arise (Todd and Marois 2004; Xu and Chun 2006; Robitaille et al. 2010).

Such anatomically distributed processing is thought to be coordinated and integrated by large-scale interareal neuronal synchronization (Siegel et al. 2012; Fries 2015; Womelsdorf and Everling 2015). Large-scale neuronal synchronization and phase coupling of neuronal oscillations in source-reconstructed magnetoencephalography (MEG) studies have indeed been shown to underlie coordination of visuospatial attention (Siegel et al. 2008; Doesburg et al. 2016; Lobier et al. 2017) and VWM (Palva et al. 2010). However, both the functional significance of large-scale neuronal synchronization in MOT tasks and, in particular, its possible role in individual attentional capacity has remained poorly understood.

We have previously shown using source-reconstructed MEG that the amplitude of gamma (γ, 30–120 Hz) oscillations is load-dependently increased in PFC, PPC, and visual areas in both MOT (Rouhinen et al. 2013) and VWM (Palva and Palva 2011) tasks and that this increase is correlated with individual VWM capacity. Furthermore, in these data, the individual capacity limitations of VWM were also predicted by concurrent large-scale high-alpha- (hα, 10–14 Hz,) and beta- (β, 14–30 Hz) band phase synchronization (Palva et al. 2010) as well as by crossfrequency phase synchronization (CFS) of these networks (Siebenhühner et al. 2016). In the present study, we address whether large-scale synchronization could play a role in the integration and coordination of neuronal processing underlying attention divided to multiple concurrently tracked visual objects and contribute to setting the individual attentional capacity limits.

We posited that the capacity of visual attention in MOT tasks would be associated with long-range synchronization of visual and frontoparietal attention networks (FPN) as well as by their crossfrequency (CF) interactions. To test this in a data-driven approach, we recorded concurrent M/EEG during a MOT task (Fig. 1a) and used the source-modeled data to identify large-scale synchronized networks and their correlation with psychophysical performance and individual attentional capacity.

Methods

The experiment used in this study is the same as described in (Rouhinen et al. 2013). MEG data were collected from 23 additional subjects. All data, if not stated otherwise, have been analyzed with a LabVIEW software (National Instruments) with customized code. This code is available upon request. An overview of the workflow is given Supplementary Figure 1.

Subjects and Recordings

A total of 42 healthy volunteers were recorded with concurrent MEG (306 channels), electroencephalography (EEG) (60 channels), electro-oculography (EOG) (horizontal and vertical channels), and electromyography (abductor/flexor pollicis brevis, or thumb channels) by Vectorview (19 subjects, sampling rate 600 Hz) and Triux (23 subjects, sampling rate 1000 Hz) M/EEG systems (Elekta-Neuromag) at the BioMag Laboratory, Helsinki University Hospital. Individual T1-weighted MRI images were recorded with a 1.5 T scanner (Siemens, Germany) using a MP-RAGE protocol at a resolution of $1 \times 1 \times 1$ mm resolution. After removing one subject whose performance was very poor, 41 subjects remained (22 females, 29 ± 6.5 years). The study was approved by the Ethical Committee of the University of Helsinki and performed according to the Declaration of Helsinki. Written informed consent was received from each subject prior to the experiment.

Tasks and Stimuli

The subjects performed a MOT task in which they attended and tracked moving visual objects and responded to feature-changes in their shape. We used LabVIEW to generate the stimuli and tasks. We recorded two variations of the task. The first task (T1) was a general attention task, where subjects tracked all objects on the screen with the object load varying from one to four. The second task (T2) was an object-selective attention task, where the object load remained at four but subjects attended and tracked only one to four objects with one color while ignoring the objects with another color (pink and yellow, respectively, Fig. 1a). The interstimulus interval between target events was 0.7–5 s. The target event was a shape change of the target object and had a duration of 100 ms. Each of the four load conditions had 160 trials in both tasks for a total of 1280 trials. The experiment was divided into eight 10 min blocks. After artifact rejection and equalizing between conditions, 124.3 ± 22.87 (mean $\pm$ SD) trials remained in T1 and 115.8 ± 29.81 in T2 for each attentional load per subject. The projected display's vertical size was 10° and the moving objects' size was 0.8°. The subjects were instructed to look at the center-of-mass of the targets and avoid saccades between targets.

Analysis of Behavioral Data

Target events were defined as "detected" if the subject responded with a thumb twitch between 200 and 700 ms from the onset of the target event and as missed otherwise. Reaction time (RT) was computed as onset of thumb twitch minus onset of target event and hit rate (HR) as the fraction of detected events (Supplementary Figure 1d). Capacity (C) was computed as $C = ((HR_{T1,L3} + HR_{T2,L3}) * 3 + (HR_{T1,L4} + HR_{T2,L4}) * 4)/4$, where T1 and T2 indicate tasks 1 and 2, respectively, and L3 and L4 the attentional loads of three and four objects, respectively, so that at 100% accuracy in all load conditions capacity would be 3.5. The subjects were divided by their capacity into three groups: high, middle, and low capacity. High-capacity subjects had capacity values ranging from 2.62 to 2.96 (mean $\pm$ SD, 2.76 ± 0.12), middle-capacity subjects values ranging from 2.01 to 2.54 (2.23 ± 0.18), and low-capacity subjects values ranging from 1.12 to 2.01 (1.55 ± 0.31). The subjects that were included in (Rouhinen et al. 2013) were classified similarly in the new current analysis except for a single subject whose classification was changed from low to middle capacity. The individual performance and capacity classification of the subjects are shown in Supplementary Figure 2.

Performance differences between loads and tasks were evaluated with both frequentist and Bayesian repeated measures ANOVA. Inverse Bayesian factors were calculated with JASP

(JASP Team 2016) to provide an estimate of evidence for the performance differences. Uninformative priors were used in non-posthoc Bayesian testing. BF_{10} gives the odds ratio for the alternative and null hypotheses given the data, and BF_{21} the odds ratio for alternative with interaction/alternative without interaction. Dimensions that had statistically significant differences in the two-way repeated measures ANOVA were further analyzed with posthoc *t*-tests. Frequentist posthoc tests were Holm-Bonferroni corrected. Bayesian posthoc tests were corrected for multiple testing by fixing to 0.5 the prior probability that the null hypothesis holds across all comparisons (Westfall et al. 1997).

Analysis of Eye Motions

Eye motion differences between different load conditions were estimated using the same trials as in synchrony analyses. Eye motions were estimated using broad-band filtered (1–120 Hz) amplitude of the horizontal and vertical EOG channels (eye motion index, EMI) and the amplitude of the derivative of eye motion (saccadic motion index, SMI). Two-way repeated measures ANOVA load × task of eye motions was used to estimate eye movement differences between load conditions and tasks. Both frequentist and Bayesian ANOVAs were used. Dimensions that had statistically significant differences in the two-way repeated measures ANOVA were further analyzed with posthoc *t*-tests. Frequentist posthoc tests were Holm-Bonferroni corrected. Bayesian posthoc tests were corrected for multiple testing by fixing to 0.5 the prior probability that the null hypothesis holds across all comparisons (Westfall et al. 1997). Correlations between eye movements and capacity were estimated with Spearman's correlation test to check if capacity groups have differences in their eye motions. Similarly to how the capacity value is calculated, the average eye motion measures of loads three and four were used in the Spearman's correlation test.

Preprocessing of M/EEG Data

Maxfilter software (Elekta Neuromag) (Gramfort et al. 2014) was used to suppress external noise (temporal signal space separation), interpolate bad channels, and colocalize recordings in signal space in MEG sensors (Supplementary Figure 1b). Fieldtrip MATLAB toolbox (MathWorks) (Oostenveld et al. 2011) was used for independent component analysis (ICA) to remove components corresponding to eye movements, heartbeat, and muscle artifacts, as well as activities with a single-channel focus in spatial distribution, or with greatest power spectral density in frequencies over 40 Hz. Time series data were then filtered into narrow-band time series using a bank of 34 complex Morlet wavelets with the time–frequency compromise term $m = 5$ and approximately log-linearly spaced center frequencies ranging from 3 to 120 Hz with exact frequencies optimized to yield as many integer–ratio frequency pairs for the analysis of CF coupling (CFC) with as few wavelet filters as possible (Palva et al. 2005; Siebenhühner et al. 2016). After filtering, the time-series data were downsampled to sampling rate of five times the center frequency.

Source Modeling and Cortical Parcellation

Anatomical reconstruction and parcellation with the Destrieux atlas from MRI images (Fischl et al. 2004; Destrieux et al. 2010)

was performed using Freesurfer (http://surfer.nmr.mgh.harvard.edu). Source modeling with minimum norm estimate using the dSPM method was carried out using MNE software (http://www.nmr.mgh.harvard.edu/martinos/userInfo/data/sofMNE.php) (Dale et al. 2000; Gramfort et al. 2014). Noise covariance matrices were computed using preprocessed broad-band filtered M/EEG time-series from 5 s time-windows taken with 5 s intervals and then used to compute one inverse operator per subject (200–250 Hz). Only time-windows that were not contaminated by eye blink or eye movement artifacts were used for noise covariance matrix computations. The source models had dipole orientations fixed to pial surface normals and a 7-mm interdipole separation throughout the cortex, yielding 5189–8054 source vertices. Single source narrowband complex vertex time series were collapsed into parcel time series with a source-reconstruction-accuracy- (fidelity-) optimized collapse operator (Korhonen et al. 2014). This optimization was done to enhance the possibility of detecting true connections among the spurious connections, see (Siebenhühner et al. 2016) for further details. We used a 400-parcel parcellation that was obtained by iteratively splitting the largest parcels of the Destrieux atlas along their most elongated axis using the same parcel-wise splits for all subjects (Palva et al. 2010, 2011). The 400-parcel data were collapsed to a coarser 200-parcel parcellation before computing interaction metrics to reduce the effects of intersubject functional variability. Parcels were also assigned functional labels based on Yeo's seven-parcel scheme (Fig. 2b) (Yeo et al. 2011). These steps refer to Supplementary Figure 1a–c.

Analysis of Interareal Synchronization

To identify cortex-wide phase-synchrony networks, we computed individual parcel-to-parcel phase-synchronization for each condition and frequency in a time window from −700 to –200 ms before target events (pretarget period) (Supplementary Figure 1e). Phase-synchronization was estimated using imaginary part (iPLV) of the complex phase-locking value (cPLV) (Palva et al. 2005). cPLV was defined as:

$$\text{cPLV} = \frac{1}{N} \sum_{n=1}^{N} \left[e^{i(\theta_p(n) - \theta_q(n))} \right]$$

where N is the number of samples and θ_p and θ_q are the phases of the time series of parcels p and q; and iPLV = |im (cPLV)|. iPLV is insensitive to zero-lag interactions and hence yields neither artificial nor true zero-lag or near-zero lag couplings (Nolte et al. 2004; Vinck et al. 2011; Palva et al. 2018; Wang et al. 2018).

Analysis of Local Oscillation Amplitudes

To investigate the modulation of local oscillations amplitudes, we used the 34 complex Morlet wavelets to compute amplitude envelopes for each wavelet frequency for each parcel P across trials N and samples T: $A_P = \frac{1}{N \times T} \sum_{n,t} A(P, n, t)$. The same −700 to –200 ms pre-target time data were used as for the synchronization analysis. Correlation of the load-dependence of amplitude with individual attentional capacity was obtained by computing the correlation between individual capacity and the change in oscillation amplitude from loads 2 to 4 with Spearman's rank test ($P < 0.05$, corrected) (Fig. 4). Significant differences in the amplitudes between detected and undetected targets were obtained using *t*-tests ($P < 0.05$, corrected). Amplitude data were

visualized per parcel on cortical surfaces as the fraction of statistically significant amplitude differences in frequency dimension at frequency band selection (Fig. 4), and per frequency as a fraction of statistically significant differences in parcel space.

Statistical Analyses

We used a data-driven large-scale data-analysis approach in the assessment of both the MEG findings and the relationships between MEG (phase coupling, amplitude, and CFC) and behavioral (such as attentional capacity) data (Brunton and Beyeler 2019). In order to not bias the data-analysis with a priori defined frequency bands, we performed the analyses on all of them and then identified the frequency bands where the relationships were the strongest, and visualized the networks for these frequency bands. Group statistics were performed separately for each frequency to identify significant interareal or parcel–parcel interactions. We tested for significant differences in the strength of synchronization between detected and undetected targets using t-tests ($P < 0.05$) and with load conditions of two or three objects, which had adequate numbers of both detected and undetected events (Fig. 2, Supplementary Figure 1g). Correlations of the strength of synchronization with attentional load, that is, with the number of to-be attended objects was estimated using Spearman's rank correlation tests ($P < 0.05$) for attentional loads of 2–4 (Fig. 3a, Supplementary Figure 1h). To estimate in which frequencies the two tasks differed, we used a two-way repeated measures ANOVA for attentional loads of 2–4 (Load $\times$ Task, $P < 0.05$, Fig. 3a). To estimate differences in the strength of load-dependent synchronization and their correlation with capacity, we computed the correlation (Spearman's rank test, $P < 0.05$) between capacity and the increase of strength of synchronization from loads 2 to 4 for phase synchrony (Figs 3b and 4), for interareal CF interactions (Fig. 5), and for local oscillation amplitudes (Fig. 4). Task differences between higher and lower capacity subjects at single target loads (2 and 3) were estimated with t-tests ($P < 0.05$, T2–T1).

We accounted for multiple statistical comparisons in two steps: the false discovery rate was reduced by removing as many of the least significant positive and negative findings as predicted by the alpha-level. We then estimated a threshold Q to define a joint probability, P', for the number of significant observations that could arise by chance in any of the frequencies of the connection density spectrum. In the interpretation and network visualization stages, only the observations exceeding the Q threshold are considered. For the 1:1 interareal synchrony, threshold Q of significant observations remaining after false discovery correction was estimated to correspond 0.672% connection density at 0.001 chance level. This threshold was used for the t-tests and Spearman's correlation tests in analyses of interareal synchrony (Figs 2a and 3). Connection density values for load effects were further normalized to a zero mean. For ANOVA analyses, a threshold of 0.475% connection density was used, which corresponded to 0.05 chance level (Fig. 3a).

Analysis of Crossfrequency Coupling

To estimate the interactions across distinct frequencies, we computed two forms of CFC: phase–amplitude coupling (PAC) and CFS. We calculated both interareal CFC among all parcel pairs p and q of the 200 parcels, and local CFC, where $p \neq q$. We estimated n:m CFS, where the integers n and m define the frequency ratio so that $n \cdot f_{\text{high}} = m \cdot f_{\text{low}}$ with values $n = 1$ and $m \in \{2,3,4,5,6,7,8\}$ using the PLV:

$$\text{PLV}_{p,q,n:m,f_{\text{low}},f_{\text{high}}} = \frac{1}{N} \left| \sum_{r,t} \exp\left[i \cdot \left(m \cdot \theta_p\left(r,t,f_{\text{low}}\right) - n \cdot \theta_q\left(r,t,f_{\text{high}}\right)\right)\right] \right|$$

where i is the imaginary unit, $N = N_r \cdot N_t$, where N_r is the number of trials r and N_t is the number of samples t within a time window, θ_p and θ_q are the phases of parcel p and q, respectively (Tass et al. 1998; Palva et al. 2005; Siebenhühner et al. 2016; Siebenhühner et al. 2020). Frequency pairs were chosen so that the ratio of their center frequencies lay within 5% deviation of the desired integer 1:m ratio.

We estimated PAC by computing the PLV between the phase of the slow oscillation and the phase of the amplitude envelope of the fast oscillation filtered at f_{low}. PAC was thus defined as:

$$\text{PAC}_{p,q,f_{\text{low}},f_{\text{high}}} = \frac{1}{N} \left| \sum_{r,t} \exp\left[i \cdot \left(\theta_p\left(r,t,f_{\text{low}}\right) - \theta_q^E\left(r,t,f_{\text{low}},f_{\text{high}}\right)\right)\right] \right|$$

where $\theta^E(t, f_{\text{low}}, f_{\text{high}})$ is the phase of the filtered amplitude envelope time series $E(t, f_{\text{low}}, f_{\text{high}})$ that was obtained by filtering $A(t, f_{\text{high}})$ with the Morlet wavelet $w(t, f_{\text{low}})$:

$$E\left(t, f_{\text{low}}, f_{\text{high}}\right) = A\left(t, f_{\text{high}}\right) \otimes w\left(t, f_{\text{low}}\right).$$

In order to correct for potentially spurious observations of interareal PAC and CFS arising from nonsinusoidal or non-zero-mean signals (Lozano-Soldevilla et al. 2016), we used a novel method based on graph theory (Siebenhühner et al. 2020). The rationale, in brief, is that interareal CFC can only be spurious if the signal at f_{low} in p and the signal at f_{high} in q are also connected otherwise, namely by local CFC and interareal synchronization between p and q. Thus, observations of interareal CFC were discarded if we observed either significant local f_{low}: f_{high} CFC in p and significant interareal synchronization at f_{high}, or significant local f_{low}: f_{high} CFC in q and significant interareal synchronization at f_{low}.

Correlation of the load-dependent synchronization with individual attentional capacity was obtained by computing the correlation between individual capacity and the increase of strength of CFS and PAC from loads 2 to 4 for phase synchrony with Spearman's rank test for interareal CF interactions (Fig. 5), and for local CF interactions.

The threshold of significant observations remaining after false discovery correction (see Statistical Analyses) was estimated by the probability, P', for a number of significant observations to arise by chance from graphs of random P-values after the false discovery reduction in any single frequency out of all wavelet frequencies. This threshold was estimated to be 0.672% connection density for the t-tests and Spearman's correlation tests in analyses of interareal synchrony, which corresponded to $P' = 0.001$ (Fig. 5). For local CFC, the threshold was 5.5% connection density at $P' = 0.001$.

Removal of Low-Fidelity Cortical Areas and Connections for Alleviating Source-Space Signal Mixing

A major limitation in connectivity analysis using M/EEG data is linear signal mixing among recorded signals that after source modeling remains as residual signal leakage among nearby parcels, which is dependent on source anatomical location and individual brain anatomy (Palva and Palva 2012). iPLV was used to estimate interareal synchronization to exclude the direct effects of zero-phase lagged linear signal mixing. Spurious interactions, however, remain even when using zero-phase lag insensitive connectivity metrics (Palva et al. 2018). Since the number of spurious interactions is dependent on the source-reconstructions accuracy, as the first step, we excluded poorly reconstructable parcel connections from the graph analysis and visualizations. We removed connections between parcels for which the source reconstruction accuracy, fidelity, was below 0.2 (2.0% of parcels) (Korhonen et al. 2014). In addition, to further exclude spurious connections, we also removed connections of those parcels that exhibited greatest signal leakage with their neighbors (fidelity radius greater than 0.3; 7.6% of connections, Supplementary Figure 1f). In total, 7.6% of all possible connections most prone to source mixing were excluded from the analyses. These sources were mostly in the deep and inferior structures (Supplementary Figure 3) as expected (Hillebrand and Barnes 2002).

Graph Analysis and Visualization

We used graph theory (Bullmore and Sporns 2009) to characterize the network structures in group-level adjacency matrices. Each thresholded adjacency matrix defined a graph made up of nodes and edges, where nodes are cortical parcels and edges are the significant interactions between nodes. Connection density (K) was used to index the proportion of significant edges from all possible interactions while degree was used to identify nodes that were central in the graphs and thus putatively played a key role in network communication. To investigate the spectral patterns of phase synchrony modulations associated with multiobject attention, we first plotted the connection density K for both the positive (K+, strengthening of interparcel synchrony) and the negative (K−, suppression of interparcel synchrony) observations as a function of frequency separately for each statistical analysis (Figs 2a and 3). Graph visualization was carried out for frequency-bands showing significant increases in phase synchrony for each condition, so that before visualization and separately for each statistical contrast, neighboring narrow-band frequencies were grouped with hierarchical agglomerative clustering by their adjacency-matrix (edge) similarity (Palva et al. 2010). Frequencies that formed clusters and had connection densities above threshold at some of the clustered frequencies were visualized.

For each selected frequency band, we first constructed a single graph by summing the adjacency matrices of each filter frequency in the band. We then selected most central connections and nodes based on their degree. To further alleviate the contribution of the remaining spurious edges ('false' interactions) created by the concurrent presence of a true interaction and linear mixing (Palva and Palva 2012; Palva et al. 2018), we then applied an edge-bundling approach (Wang et al. 2018). In this approach, edges that had high linear mixing were bundled into hyperedges. Only hyperedges consisting of

at least six edges were visualized to decrease the false positive rate and reduce visual clutter.

Correlation of Amplitudes and the Strength of Synchronization

To test whether changes in signal-to-noise ratio (SNR) by changes in the strength of oscillations amplitudes could be correlated with modulations in the strength of synchronization, we first normalized oscillation amplitudes and mean node strengths within subjects. The normalized amplitude and node strength were correlated with Spearman's correlation test ($P < 0.05$, corrected), either across frequency bands with all parcels or per parcel.

Results

Psychophysics

To assess the effect of attentional load on behavioral performance, we estimated HR and RT in the responses to the target objects. Subjects' performance was similar in tasks T1 and T2 and with increasing load, HR decreased and RT increased (Fig. 1b). Two-way repeated measures ANOVA for HR had a significant main effect of load ($F(1.188, 47.503) = 148.165$, $P < 0.001$; $BF_{10} = 1.929e + 76$, with Greenhouse-Geisser correction because Mauchly's test indicated sphericity violation; $P < 0.001$, $\varepsilon = 0.396$), but neither a main effect of task ($P = 0.111$; $BF_{10} = 0.166$) nor an interaction effect ($P = 0.074$; $BF_{21} = 0.392$). Similarly to HR, also RT showed a significant main effect of load ($F(2.026, 81.043) = 127.888$, $P < 0.001$, with Greenhouse-Geisser correction because Mauchly's test indicated sphericity violation; $P < 0.001$, $\varepsilon = 0.675$; $BF_{10} = 5.871e + 54$) and no main effect on task ($P = 0.550$; $BF_{10} = 0.139$) or an interaction effect ($P = 0.360$; $BF_{21} = 0.198$). Posthoc tests showed significant differences in HR between all loads (ranges of tests between 1 and 4 loads: $t = 6.033–14.337$, $P < 0.001$, Holm-Bonferroni corrected, posterior odds $= 2.639e + 4 − 1.021e + 26$). Posthoc tests also showed significant differences in RT between all loads (ranges of tests between 1 and 4 loads except 3 and 4: $t = −13.286$ to 5.068, $P < 0.001$, Holm-Bonferroni corrected, posterior odds $= 3.369e + 7 − 1.021e + 26$), with the difference between loads 3 and 4 being small ($t = −2.584$, $P = 0.014$, Holm-Bonferroni corrected, posterior odds $= 2.158$).

Eye Motion Differences Between Loads and Subjects

As the tasks required tracking of moving visual objects, eye-movements might differ between attentional loads. To investigate the putative differences in the frequency of eye motions between tasks and different target loads, eye motions were estimated from EOG data using an EMI. EMI measures saccades and smooth pursuit eye motions, with more eye motions meaning greater EMI. EMI was different between attentional load 1 and loads 2–4, but not between loads 2–4 (Fig. 1c). Two-way repeated measures ANOVA of EMI showed a significant main effect of load ($F(3, 120) = 24.811$, $P < 0.001$; $BF_{10} = 7.844e + 18$, no Mauchly's sphericity violation), but no main effect of task ($P = 0.068$; $BF_{10} = 0.477$) nor an interaction effect ($P = 0.569$; $BF_{21} = 0.805$). Posthoc tests on load between one target and multiple targets showed more eye movements for multiple targets compared with single target (ranges of 1 vs. 2, 3, or 4: $t = −5.582–5.091$, $P < 0.001$, Holm-Bonferroni corrected, posterior odds $= 5.466e + 6 − 1.161e + 8$). Posthoc tests on load between multiple targets showed strong evidence against
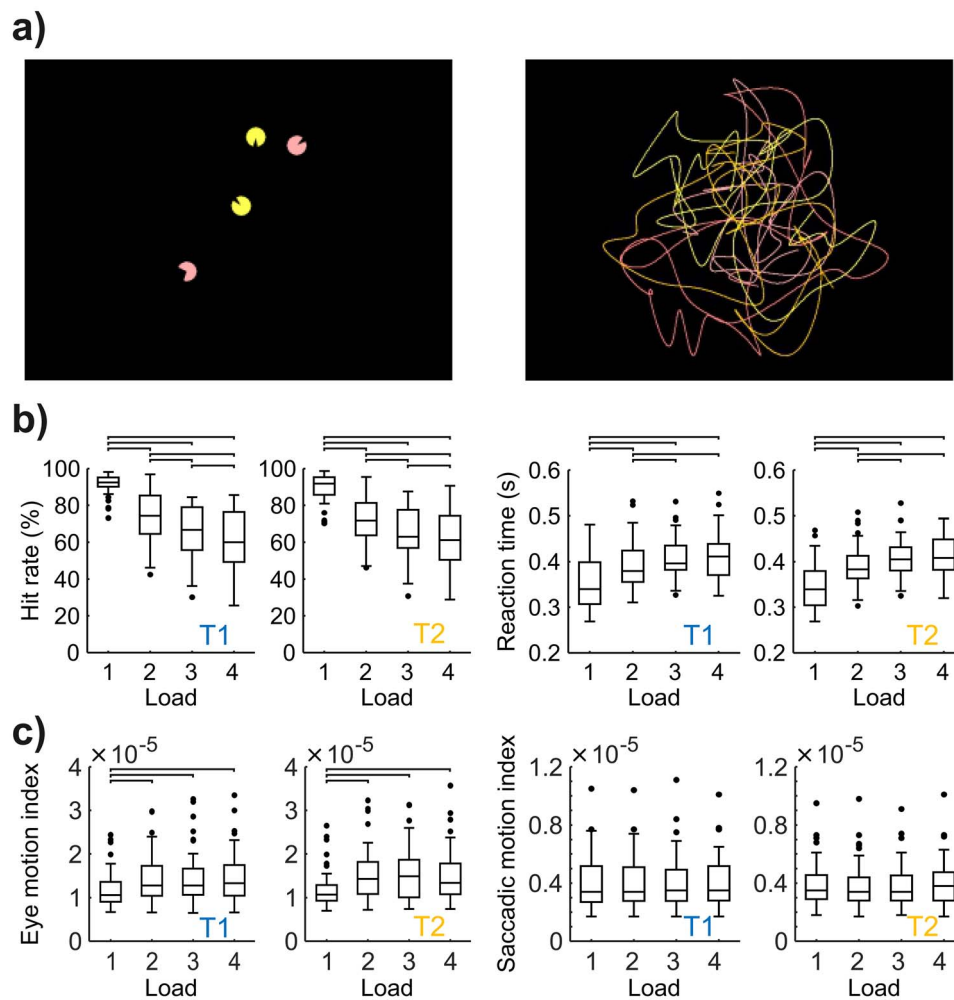
Figure 1. The schematics of the experiment and psychophysical performance. (*a*) Left: An example frame of Task 2 with two pink targets and two yellow distractors. The leftmost object shows a target event. Right: Example of paths of the objects during 45 s. (*b*) Boxplots of HR and RT for Task 1 (T1) and Task 2 (T2). (*c*) Boxplots of eye and saccadic motion indices for T1 and T2. In boxplots, median is marked with a line, and the whiskers extend at maximum to 1× the interquartile range. Lines above represent significant differences between loads (P < 0.01, Holm-Bonferroni corrected posthoc *t*-tests).

differences in EMI between the multiple loads (ranges of 2 vs. 3 or 4, or 3 vs. 4: $t = -0.026$–0.575, $P = 1.000$, Holm-Bonferroni corrected, posterior odds $= 0.050$–0.062). To exclude the potential confounder of eye-movements in the synchronization analyses, we therefore used loads 2–4 for subsequent data-analyses. SMI showed no difference between tasks or different loads (Fig. 1*c*). Two-way repeated measures ANOVA of SMI had no significant effects (most significant of load, task or interaction effects: $F(3, 120) = 1.496$, $P = 0.219$; $BF_{10} = 1.683$). The attentional capacity was inversely correlated with EMI, with lower capacities being associated with greater EMI (Spearman's correlation T1: $r = -0.49$, $P = 0.001$, T2: $r = -0.48$, $P = 0.001$) as well as with SMI with a marginal negative correlation (Spearman's correlation T1: $r = -0.27$, $P = 0.082$, T2: $r = -0.17$, $P = 0.276$).

Large-Scale Network Synchrony is Correlated with Target Detection

We first asked whether increased strength of pretarget synchronization would predict the detection of target events by estimating all-to-all phase synchronization among cortical parcels for frequencies from 3 to 120 Hz in a 0.5 s time window preceding the target events (-0.7 to -0.2 s). We assessed whether synchronization of the detected target events was stronger compared with that of the undetected events (*t*-test loads 2 and 3, $P < 0.05$, corrected). In T1, the strength of theta (θ, 3–4.4 Hz) and gamma (γ, 45–66 Hz) synchronization, and in T2, the strength of alpha (α, 7–9 Hz) and γ (45–51 Hz) band phase synchronization were increased if the target events were subsequently detected compared with when they were not detected (Fig. 2*a*). In contrast, synchronization in the 30–40 and 70–80 Hz γ-bands was suppressed in T2. We next plotted the most significant connections of the networks of which strength were increased. To aid functional interpretation of the connections, we colocalized anatomical brain regions with the fMRI-based functional subsystems (Yeo et al. 2011) (Fig. 2*b*). In the θ network in T1 occipital pole, functional part of the V1, as well as superior and middle occipital gyrus (sOG, mOG) in the right-hemispheric primary, visual areas were connected to hubs in the posterior parietal cortex (PPC) with high degree hub nodes in the intraparietal sulcus (intPS) of the dorsal attention networks (DAN), and angular gyrus (iPGang) of the default mode network (DMN) (Fig. 2*c*).
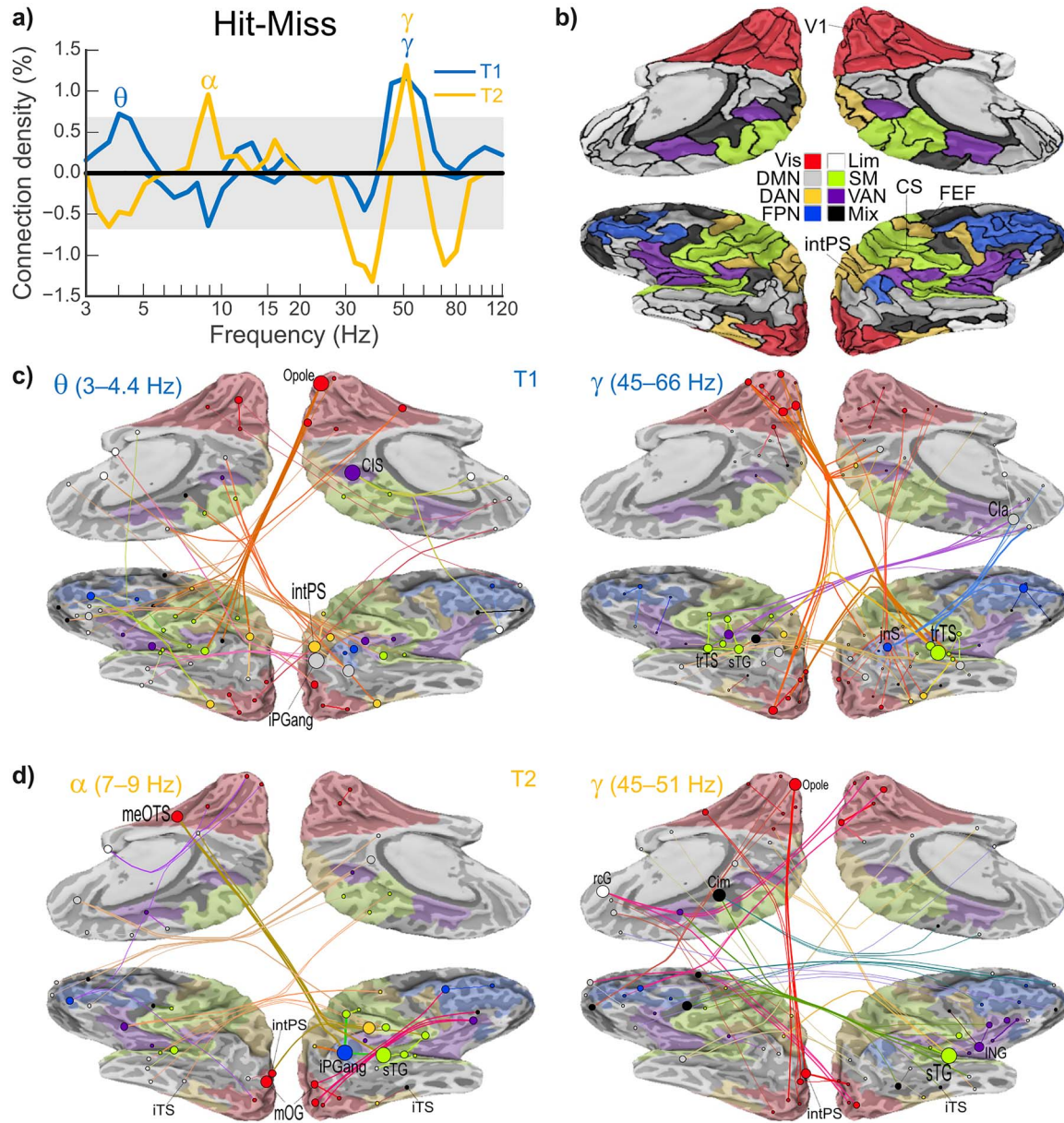
Figure 2. Large-scale synchrony differs between perceived and unperceived target events. (*a*) Difference in the strength of synchronization between perceived (Hit) and unperceived (Miss) target events estimated separately for each parcel-pair and averaged over loads 2–3. Significant difference is plotted as connection density indicating the fraction of parcels with either significant positive or negative difference in the strength of synchronization as a function of frequency. Positive values indicate significantly stronger synchrony for perceived than unperceived target events, while negative values indicate stronger synchrony for unperceived target events ($P < 0.05$, *t*-test, corrected). Note, in a given frequency, positive and negative effects can be observed concurrently in different connections. The gray shading (−0.67 to 0.67%) indicates 0.1% chance-level (See Methods). (*b*) Parcels assignments in Yeo7 parcellation (Yeo et al. 2011); visual (Vis), limbic (Lim), DMN, somatomotor (SM), DAN, ventral attention network (VAN), frontoparietal network (FPN), and non-colocalized (Mix) parcels. (*c*) Theta (θ, 3–4.4 Hz) and gamma (γ, 45–66 Hz) band networks that were stronger for perceived than unperceived target events for T1. Only the 8–10% strongest connections are shown. Vertex sizes and edge widths are relative to node degree. Networks are visualized on an inflated cortical surfaces, where light areas are gyri and dark areas sulci. (*d*) Alpha (α, 7–9 Hz) and gamma band (γ, 45–51 Hz) networks that were stronger for perceived than unperceived target events. Abbreviations: a, anterior; me, medial; int, intra; s, superior; ang, angular; pole, pole; rc, rectus; tr, transverse; jnS, sulcus intermedius primus of Jensen; CI, cingulate; T, temporal; O, occipital; G, gyrus; and S, sulcus.

The γ network, in contrast, connected visual cortices bilaterally. Additionally, it connected transverse temporal sulcus (trTS) to visual regions and nodes within the somato-motor network (SM). In T2, α-band network nodes in the right lateral occipital cortex (LOC) were connected with right anterior PFC and right LOC with left PPC the high degree hubs being angular gyrus (iPGang) and intPS (Fig. 2*d*). In contrast, γ network connected

visual regions bilaterally, similarly to T1. We did not observe significant local oscillation amplitude modulation differences between detected and undetected target events in either of the tasks (*t*-test, $P < 0.05$, corrected) (Supplementary Figure 4a) and hence the increases in oscillation amplitudes cannot explain the increases in the strength of synchronization via increased SNR.
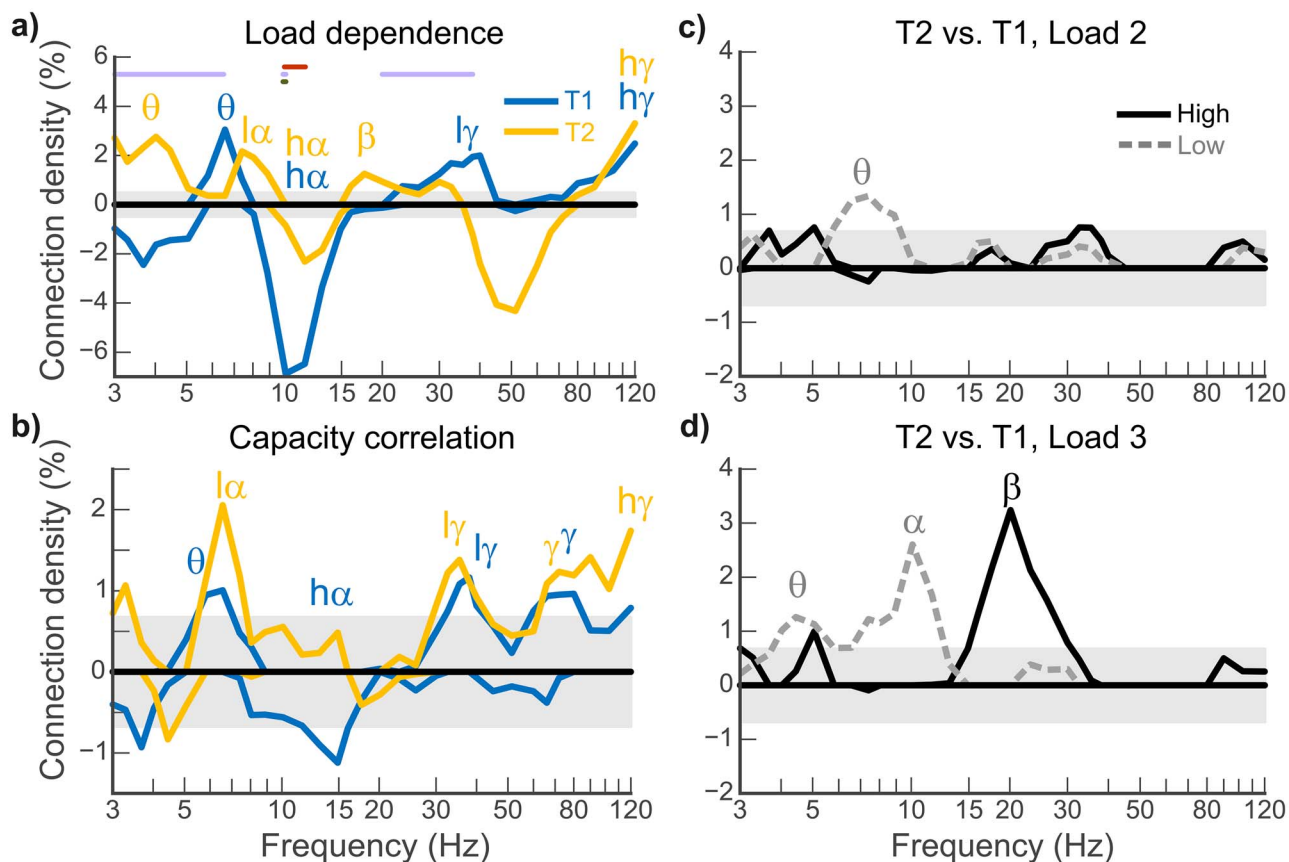
Figure 3. Load-dependence of large-scale synchrony is correlated with individual attentional capacity. (*a*) The correlation of the strength of synchronization with attentional load was estimated separately for T1 (blue) and T2 (yellow) for each parcel pair (N = 41, Spearman rank correlation tests; P < 0.05, corrected). Connection density, i.e., the fraction of connections with significant correlation, is plotted separately for positive or negative correlations as a function of frequency. Note in a given frequency, positive and negative correlations can be observed concurrently indicating the presence of these effects in different connections. Peaks in the connection density are found in theta (θ, 5–7 Hz), low gamma (lγ, 30–40 Hz) and high-gamma (hγ, > 80 Hz) bands for T1 and in low-alpha (lα, 7–10 Hz), low gamma and high-gamma bands in T2. Red lines indicate frequencies with the main effect of load, violet with the main effect of task, and green with the interaction (Two-way repeated measures ANOVA (Load × Task). (*b*) Correlation of load-dependent synchronization with individual attentional capacity estimated separately for T1 and T2 and for positive and negative tails as in *a* (N = 41, Spearman's rank correlation test, P < 0.05, corrected). Peaks in the connection density are found in theta (θ, 5–7 Hz), low gamma (lγ, 30–40 Hz) and gamma (γ, 60–80 Hz) bands for T1, and in low-alpha (lα, 7–10 Hz), low gamma (lγ, 30–40 Hz), and gamma (γ, 60–72 Hz) bands in T2. (*c*) Difference in the strength of interareal synchronization between T2 and T1 (t-test, P < 0.05, corrected) in load 2. Positive values indicate stronger synchrony in T2 than in T1. Black line indicates synchronization in high-capacity subjects, gray dashed line in lower capacity subjects. (*d*) Same as in (*c*) but for target load.

Load-Dependent Increases in Synchronization Correlate with Individual Attentional Capacity

If neuronal synchronization plays a role in the regulation of neuronal processing achieving the attentional functions during MOT tasks, it should be strengthened as a function of attentional load. We assessed whether synchronization is strengthened by attentional load (Spearman's correlation test loads 2–4, P < 0.05, corrected, reduced). We excluded load 1, because of differences in the eye movements compared with the other attentional loads (2–4) and analyzed data from loads 2 to 4 which showed no differences in eye motions (EMI or SMI). In T1, interareal synchronization was increased in θ (6–7 Hz), low-γ (30–40 Hz), and high-γ (90–120 Hz) bands but decreased in the high-alpha (hα, 10–12 Hz) band (Fig. 3a). In T2, interareal synchronization was load-dependently increased in low θ (3–4.4 Hz), low-α (7–9 Hz), β (17 Hz), and high-γ (100–120 Hz) bands and again decreased in the hα band as well as in the 40–50 Hz γ band. Two-way repeated measures ANOVA of Load × Task (P < 0.05, corrected)

showed task main effects in θ (3–6.5 Hz), α (10 Hz), and β/low-γ (20–38 Hz), load main effect in α (10–12 Hz), and an interaction effect in α (10 Hz) (Fig. 3a).

We next tested if load-dependent modulation in the strength of synchronization was correlated with individual capacity values. In both tasks, individual capacity was correlated with load-dependent increase in the strength of synchronization in θ to low-α (6–9 Hz), low-γ (33–40 Hz), and γ (66–80 Hz) bands (Spearman's correlation test, P < 0.05, corrected) (Fig. 3b). In both tasks, load-dependent increase in the strength of synchronization was observed in high-capacity subjects in θ (6–7 Hz), low-γ (36 Hz), and high-γ (90–120 Hz) bands (Supplementary Figure 5). In contrast, low-capacity subjects only showed increased load-dependent synchronization in β (15–23 Hz) band in T1, and θ (4–5 Hz) band in T2.

T1 and T2 differed in the demand to suppress irrelevant visual information, which was necessary only in T2. We therefore further investigated if low- and high-capacity subjects had differences in synchronization patterns between T1

and T2 reflecting this demand. To this end, the strength of synchronization between T1 and T2 was compared for loads two and three separately for low- and high-capacity subjects. In low-capacity subject, θ or α band synchronization was stronger in T2 compared with T1 in both loads 2 and 3 (Fig. 3c,d). Instead in high-capacity subjects, more β (15–26 Hz) frequency band synchronization was observed in T2 than T1 in load 3, i.e., when the task was more demanding. These results hence suggested that θ, α, and β band oscillations all contribute to the suppression of irrelevant visual objects albeit differently in low- and high-capacity subjects.

Network Synchronization Among Visual and Frontoparietal Regions are Correlated with Attentional Capacity

One of the major goals was to investigate in which brain networks the strength of synchronization preceding the target event would be correlated with variability of individual attentional capacity. To this end, we extracted the graph structures and anatomical localization of the networks exhibiting a significant interaction between attentional capacity and load-dependent synchrony. In θ and α bands, the strength of long-range connections between visual cortex and PFC correlated with capacity, and in T2 also the connections between visual cortex and PPC (Fig. 4a,b). The network synchronization in the θ/α was independent of the local oscillation amplitude modulations, which were not correlated with capacity. Also in low-γ (lγ) band, the strongest connections correlated with individual attention capacity were in the visuo-frontal network in T1. In T1, capacity was correlated with the strength of connections in the SM network connected to PPC and PFC. In addition to synchronization, also local increases in oscillation amplitudes were correlated with individual attention capacity. In SM and PFC, the major hubs were indeed colocalized with increases in oscillations amplitudes indicating that large-scale synchronization connected the local γ activity across these cortical areas. However, intPS and nodes in the visual cortex were independent of the increases in the amplitude of oscillatory activity indicating the presence of phase-coupling in the absence of global power effects. In T2 in low-γ band, capacity was correlated with the strength of connections in the SM network connected to PPC and PFC. In the higher γ band (60–80 Hz), connections that correlated with individual attentional capacity connected primary visual regions and LOC bilaterally and these visual regions to PFC in both tasks. As for low-γ band, SM nodes were colocalized with oscillation amplitudes, while nodes in PFC, PPC or visual cortex were not. Similar network organization was also found for high-γ network that was correlated with attentional capacity only in T2 (Supplementary Figure 6).

Correlation of Synchronization with Oscillation Amplitudes

To explicitly test the correlation between the strength of interareal synchronization and oscillation amplitudes and whether the increases in synchronization were explained by the increase in the SNR caused changes in the strength of the oscillation amplitudes, we estimated the correlation between parcels' amplitudes and their mean node strengths (Spearman rank correlation test, $P < 0.05$, FDR corrected). In both tasks, the strength of synchronization and oscillation amplitudes were

very weakly correlated (Supplementary Table 1). The correlations ranged from $-0.162 < r < 0.219$ (mean 0.102) in T1, and from $-0.027 < r < 0.296$ (mean 0.148) in T2 when the amplitude and node strength values were estimated within frequency bands (Supplementary Table 1). The load-dependent (loads 4–2) correlations were slightly higher when estimated separately for each wavelet frequency (Supplementary Figure 7a). Weak correlation ($\sim$0.23 in both tasks) between amplitude and synchronization was observed in high α-band (10 Hz), in which synchronization was load-dependently suppressed and also in the high-γ band, in which load-dependent high γ synchronization was found. The strongest correlations were found in the temporal and occipito-temporal areas particularly in the high-γ band (Supplementary Figure 7b). These results show that oscillations amplitudes in terms of SNR do not explain modulations in the strength of oscillation amplitudes. Furthermore, the weak correlations between oscillations amplitudes and synchronization suggest that also mechanistically these phenomena are largely different, which was evident also in the lack of colocalization of oscillation amplitudes and synchronization specifically in the lower frequencies.

Interareal Crossfrequency Synchronization and Phase-Amplitude Coupling are Correlated with Attentional Capacity

In our earlier study on the amplitude effects in the present MOT data, we observed that γ-band oscillation amplitudes were positively correlated with attentional load, specifically in subjects with high attentional capacity (Rouhinen et al. 2013). We have also observed that concurrent large-scale networks in distinct frequency bands are CF-phase synchronized during a multiobject VWM task (Siebenhühner et al. 2016). Such cross-frequency couping (CFC) could underlie the integration of neuronal processing across functionally specialized frequency bands and hence support integration across neuronal processing hierarchies (Jensen and Colgin 2007; Schroeder and Lakatos 2009b; Fell and Axmacher 2011; Palva and Palva 2017).

As we here observed interareal synchronization in the MOT tasks to take place concurrently in multiple frequencies from θ to high-γ bands, we next addressed whether these oscillations would be coupled by CFC in a behaviorally relevant manner. We evaluated two forms of CFC:CF synchrony (CFS) and PAC. We estimated both local (i.e., within the same parcel) and interareal (between distinct parcels) CFS and PAC among all cortical parcels and between bands having frequency ratios from 1:2 to 1:8 (see Methods), and then tested for all parcel pairs whether the difference in CFS strength between loads 4 and 2 was correlated with subjects' individual capacity (Spearman's rank test, $P < 0.05$), as described for 1:1 phase synchronization. We further used a novel graph-theory-based method (Siebenhühner et al. 2020) to discard spurious observations of interareal CFC that can arise if there is a nonsinusoidal or non-zero-mean signal at least one of the two parcels, leading to artificial frequency components in filtering (and thus spurious local CFC) which then "spread" to the other parcel by within-frequency interareal phase synchronization (see Methods). Since this approach can only detect spurious interareal CFC, no correction for spurious local CFC was performed.

Genuine interareal CFS was significantly and positively correlated with capacity at ratio 1:2 among low-to-high γ frequencies in both T1 and T2, where a larger number of connections
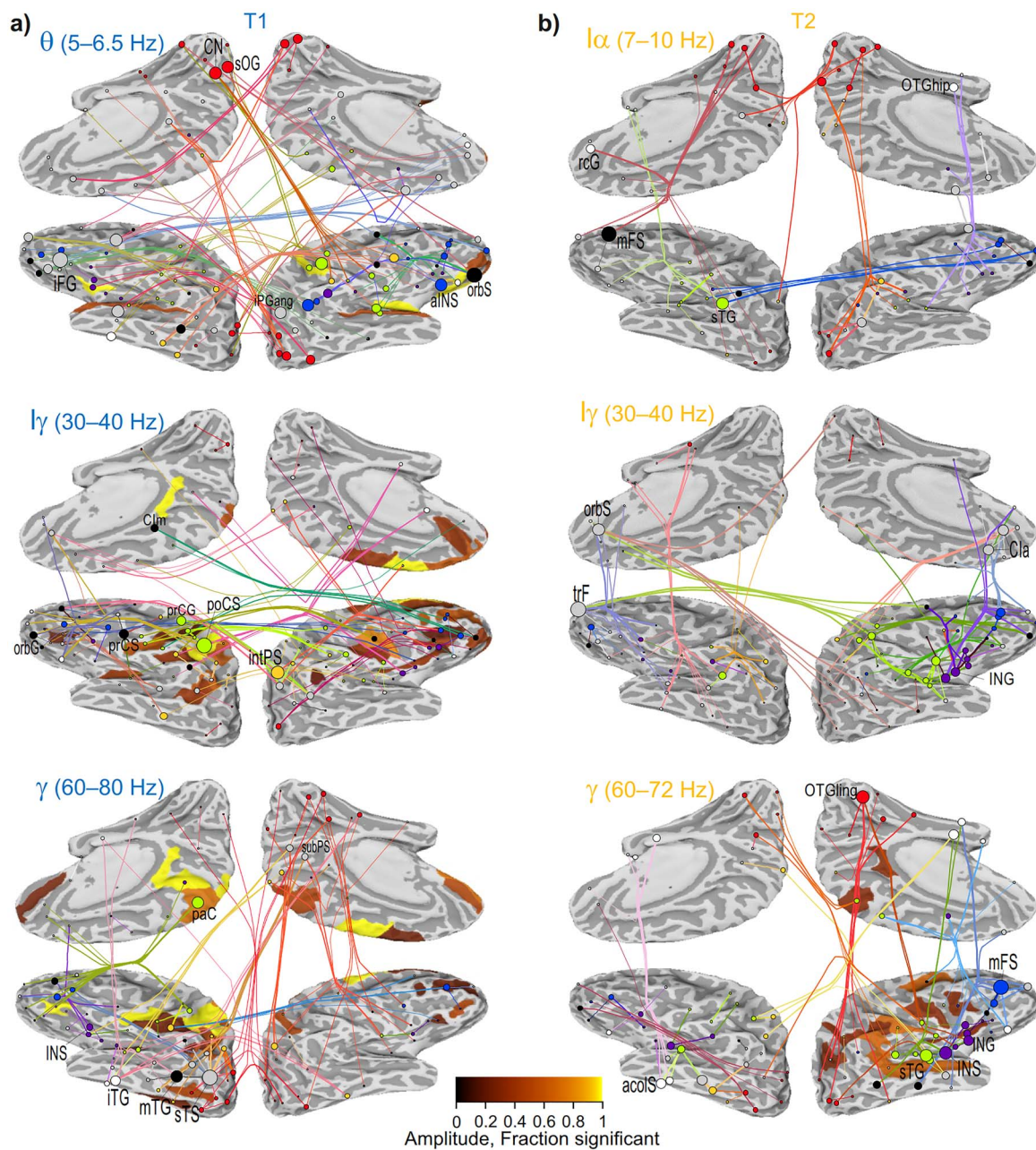
Figure 4. Graphs of load-dependent networks that are positively correlated with individual attentional capacity. (*a*) Load-dependent theta (*θ*, 5–7 Hz), low gamma (l*γ*, 30–40 Hz), and gamma (*γ*, 60–80 Hz) band networks that are positively correlated with capacity in T1. (*b*) Load-dependent low-alpha (l*α*, 7–10 Hz), low gamma (l*γ*, 30–40 Hz), and gamma (*γ*, 60–72 Hz) band networks that are positively correlated with capacity in T2. Only the 7–14% of strongest connections are shown. Color of the parcel shows that also parcel amplitudes are significantly correlated with the attentional capacity, the color indicating the fraction of significant narrow-band frequencies per parcel. The attentional capacity is predicted by theta and low-alpha band synchronization between visual cortices and PFC as well as by gamma-band synchronization between bilateral visual regions. Abbreviations: a, anterior; m, middle; i, inferior; s, superior; ang, angular; col, transverse collateral; hip, parahippocampal; int, intra; ling, lingual; orb, orbital; po, post; rc, rectus; sub, sub; tr, transverse; paC, paracentral lobule; CI, cingulate; IN, insular; F, frontal; P, parietal; T, temporal; O, occipital; G, gyrus; and S, sulcus.

than that could be expected by chance was observed (Fig. 5). Individual attentional capacity was also correlated with PAC of *β* and *γ* oscillation phases with the amplitude of high-*γ* oscillations at ratios 1:2–1:4 in both tasks. This indicates that CFC of *γ* and high-*γ* oscillations preceding target detection was correlated with good attentional capacity. Importantly, CFS of h*α* with *β*- and *γ*-band oscillations was correlated with individual attentional capacity in T1 showing that h*α* suppression was

synchronized with higher frequencies that showed increased task-dependent synchronization. Similarly, also the PAC of *α* and also *β* oscillations with higher frequencies were correlated with individual attentional capacity.

Negative correlations of CFS with individual capacity were rare in T1, and for T2 were mostly found between *θ*-band oscillations with higher frequencies. Similarly to CFS, negative correlations of PAC with capacity were observed mainly for low
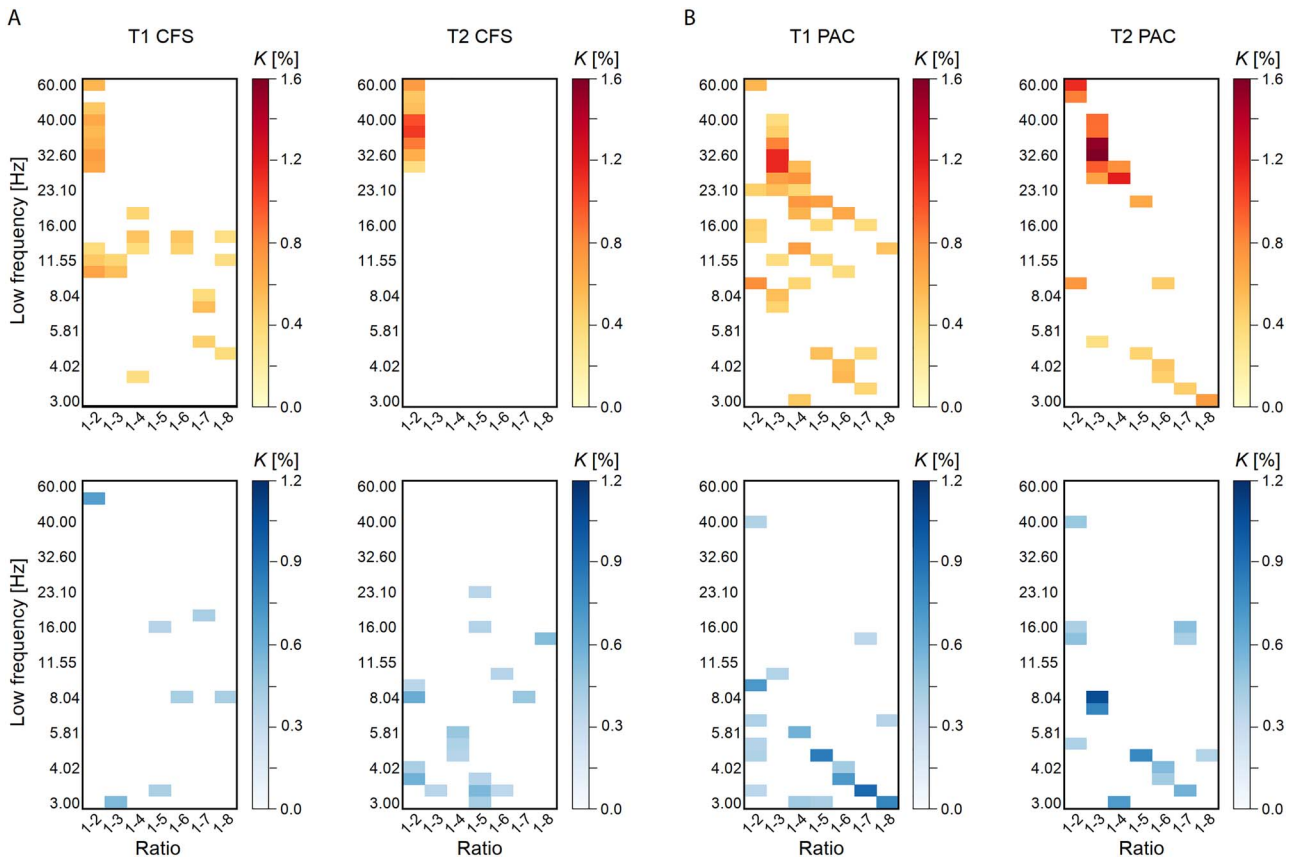
Figure 5. Correlation of load-dependent interareal CFS and PAC with attentional capacity. (*a*) Connection density (K) of CFS connections for which the increase in strength from loads 2 to 4 is positively (top row) or negatively (bottom row) correlated with individual attentional capacity. The lower frequency is displayed on the y-axis and the ratio of the coupling on the x-axis. In T1, the individual capacity was predicted by α oscillations synchronized with β and γ oscillations over ratios. In both tasks, capacity was also predicted by synchronization between γ and high-γ bands at ratio 1:2. (*b*) Same for PAC. The individual capacity was predicted by α to β oscillations phases coupled with the amplitude of higher frequency oscillations across ratios as well as by coupling of γ-oscillation phase with the amplitude of high-γ amplitudes. Negative correlations were weak for both CFS and PAC.

frequencies in the θ band and all ratios in both tasks. Positive correlations of local CFS and PAC with capacity, where a larger number of significant correlations than could be expected by chance, mostly coupled β and γ with γ and high-γ oscillations at ratios 1:2–1:6 in both tasks (Supplementary Figure 8).

Discussion

We used a well-validated MOT task (Pylyshyn and Storm 1988; Oksama and Hyona 2004; Bettencourt et al. 2011) together with M/EEG recordings to investigate whether large-scale synchronization plays a role in attention to multiple objects and whether a load-dependent modulation of synchronization would be correlated with the variability in individual attentional capacity. We found that large-scale θ-, α-, and γ-band synchronization prior to target events was strengthened when the events were detected. Good individual attentional capacity was positively correlated with load-dependent strengthening of θ-, lα-, lγ-, and γ-band synchronization was as well as with load-dependent CFC. Taken together, neuronal synchronization during attentional visual tracking was dynamically organized in a task-dependent manner and this multiscale dynamic organization of pretarget activity correlated with both intertrial and interindividual variability in behavioral performance and attentional capacity. These

findings thus constitute evidence for that both within-frequency synchronization of neuronal oscillations (Singer 2009; Fries 2015) and their CFC (Palva et al. 2005; Fell and Axmacher 2011; Jensen et al. 2014; Palva and Palva 2017) may mechanistically contribute to the integration and regulation of neuronal processing across functionally specialized brain regions to achieve attentive visual tracking.

Target Detection is Preceded by Large-Scale Theta/Alpha- and Gamma-Band Synchronization

Target detection was preceded in both tasks by large-scale γ-band synchronization as well as by synchronization of the lower frequency oscillations. While in the general attention task (T1), synchronization in the θ-band preceded successful target detection, in the object-based selective-attention task (T2), successful target detection was preceded by α-band synchronization. These data thus suggest that in addition to visuo-spatial attentional control (Doesburg et al. 2016; Lobier et al. 2017; D'Andrea et al. 2019), α-band synchronization may coordinate also object-based selective attention. Further, the increase in γ-band synchronization is in line with the idea that γ-band synchronization is related to attended stimulus perception in humans (Siegel et al. 2008).

This synchronization connected visual regions with PPC and PFC, including both DAN and then FPN (Kastner and Ungerleider 2000; Corbetta and Shulman 2002; Sadaghiani et al. 2009; Ptak 2012; Harding et al. 2015). These regions are also key regions in predicting MOT performance in fMRI (Culham et al. 1998; Battelli et al. 2001; Jovicich et al. 2001; Howe et al. 2009; Alnaes et al. 2015). Importantly, nodes in the visual cortex also included inferior temporal sulcus (iTS), which is related to object perception (Riesenhuber and Poggio 2002). These data suggest that during object-based selective attention, synchronization couples the attentional (PFC and PPC) systems with those generating the task-relevant object representations.

Load-Dependent Increase in Synchronization Correlates with High-Attentional Capacity

In line with prior MOT studies (Drew and Vogel 2008; Bettencourt and Somers 2009; Drew et al. 2011), we found large individual variability in attentional capacity. Similarly to prior observations for VWM capacity (Palva et al. 2010), the capacity of visual attention correlated with the strength of synchronization. We found here that load-dependent strengthening of synchronization in the θ and α bands, together with that in lγ- and γ-frequency bands, correlated with individual attentional capacity in both general attention (T1) and object-based selective attention (T2) tasks. Importantly, specifically strengthening of the long-range connections between visual cortex and PFC in the θ and α bands and of the connections between bilateral visual cortices in γ band was positively correlated with good attentional capacity. These results suggests that in the present task, both θ- and α-band synchronization are related to attentional top–down control in MOT task as previously suggested for visuospatial attention (Daitch et al. 2013; Harper et al. 2017; Lobier et al. 2017; D'Andrea et al. 2019) while the γ-band is related to integration of visual information (Kreiter and Singer 1996; Bosman et al. 2012; Siegel et al. 2012; Womelsdorf et al. 2012). These results are also in accordance with prior fMRI MOT studies showing that both visual cortex and PFC exhibit task-load-dependent BOLD signal increases (Culham et al. 1998; Jovicich et al. 2001) as well as with our previous findings of load-dependently increased γ-oscillation amplitudes in visual regions (Rouhinen et al. 2013).

Importantly, the capacity of VWM (Gaspar et al. 2016) and multiobject attention (Mäki-Marttunen et al. 2020) are known to be predicted not only by the ability to attend multiple objects but also by the ability to ignore distractors. We thus tested if the strength of synchronization would be correlated with the demand to suppress the processing of irrelevant visual object information. Interestingly, the strength of θ–α synchronization was associated with such suppression demands similarly to that found for local α oscillations (Jensen and Mazaheri 2010; Herring et al. 2015) albeit only in low-capacity subjects. In the high-capacity subjects, the suppression of irrelevant visual objects was correlated with the strength of β-band synchronization pointing towards a functional similarity between α- and β-band synchronization on one hand, and towards differences in functional coordination of executive processing in low- and high-capacity subjects on the other. These data are also partially in line with data from attention blink tasks, in which theta and beta band synchronization have been associated with encoding and maintenance of target events—i.e., with sustained attention whereas theta and alpha-band synchronization have been related to attentional

filtering of relevant visual information among irrelevant targets (Gross et al. 2004; Glennon et al. 2016).

Overall, our data show that attentional capacity is limited both by the coupling of visual cortices—essential for representation of visual information (Riesenhuber and Poggio 2002; Grill-Spector and Malach 2004; Sayres and Grill-Spector 2008; Vinberg and Grill-Spector 2008)—with the PPC and PFC associated with attention top–down control (Spadone et al. 2015; Meehan et al. 2017). Interareal synchronization of neuronal oscillations played a role in both the efficacy of visual information integration and the suppression of irrelevant objects.

Individual Attentional Capacity is Correlated with the Strength of Crossfrequency Coupling

A pervasive feature in the present results was the concurrent presence of multiple networks at distinct frequencies, which implies that also CFC might be relevant to MOT task performance. CFC has been proposed to underlie the integration and coordination of neuronal processing across functionally specialized frequency bands (Jensen and Colgin 2007; Schroeder and Lakatos 2009b; Fell and Axmacher 2011; Palva and Palva 2017). Many prior studies have found PAC to couple fast and slow oscillations during VWM (Sauseng et al. 2009; Axmacher et al. 2010; Bahramisharif et al. 2018). We have previously shown that functional integration of fast and slow oscillatory networks during multiobject VWM may also be achieved by interareal CFS (Siebenhühner et al. 2016). As multiobject attention tasks and VWM tasks share many similarities both at the cognitive (Pylyshyn and Storm 1988; Luck and Vogel 1997; Cowan 2001; Cowan et al. 2005; Treisman 2006; Bettencourt et al. 2011) and at the electrophysiological (Vogel and Machizawa 2004; Vogel et al. 2005; Drew and Vogel 2008; Drew et al. 2011, 2012; Lapierre et al. 2017) levels, in the present study, we investigated if either interareal CFS or PAC were correlated with multiobject attentional capacity. To ensure that our observations of CFC were not spurious, we use a novel graph-theory-based method to remove putatively spurious connections (Siebenhühner et al. 2020).

We observed that indeed, load-dependent increases in interareal CFS as well as PAC between low- and high-γ bands were positively correlated with attentional capacity in both tasks, albeit with slightly different spectral profiles. This finding suggests that individual attentional capacity is dependent on functional integration of γ and high-γ oscillations. In the prior analyses of the present data, specifically load-dependent γ oscillations characterized neuronal activity in subjects with high attentional capacity (Rouhinen et al. 2013). Our result now shows that these γ oscillations are nested with each other in large-scale networks.

Crucially, hα oscillations were CF synchronized with β and γ band oscillations, this coupling before target onset predicting good attentional capacity in T1. Hα oscillations that were CF coupled with higher frequencies were, however, suppressed by the load this suppression being significantly correlated with capacity in T1. Similarly, also the PAC of α and also β oscillations with higher frequencies were correlated with individual attentional capacity. These data support the hypothesis that in addition to underlying top–down attention control, theta and α oscillations provide temporal frames for attended visual perception (Jensen et al. 2014; VanRullen 2016; Palva and Palva 2018; Lakatos et al. 2019). However, we found no evidence for that similar mechanisms would operate for object-based selective visual attention task. Together with significant, albeit weak, negative

of correlation of CFS and PAC of θ band oscillations with higher frequencies, these data also show that α and γ oscillations are anticorrelated through dynamical CFC and uncoupling. Thus, overall, CFS and PAC are behaviorally significant CFC mechanisms in visual attention and may support the regulation of neuronal processing across frequencies (Palva et al. 2005; Jensen and Colgin 2007; Palva and Palva 2007, 2017; Axmacher et al. 2010; Canolty and Knight 2010; Voytek et al. 2010).

Relationship to VWM

We found here that the anatomical and spectral patterns of synchronization as well as CFC are correlated with individual attentional capacity in MOT tasks. These data suggest that subjects with high-attentional capacity exhibit stronger and more efficient coordination of neuronal processing among representational and executive brain regions. These findings parallel those observed earlier with a comparable delayed match-to-sample VWM task (Palva et al. 2010; Siebenhühner et al. 2016), which provides further neurophysiological evidence for that VWM and visual attention share partially overlapping neuronal mechanisms (Cowan 2001; Cowan et al. 2005). In the current MOT task, attentional capacity was positively correlated with strength of synchronization in lα- (7 Hz) and γ-band phase synchronization in both tasks. This finding is similar to that in VWM, where the strength of α- and β-band synchronization was increased by the load and predicted individual VWM capacity limits (Palva et al. 2010). In contrast with the VWM, however, hα-band synchronization in the present MOT task was suppressed in a manner correlated with individual attentional capacity. This distinction of α oscillations between VWM and attention supports the idea that α oscillations are related to internal, self-oriented processing being enhanced in VWM and suppressed in visual attention (Klimesch et al. 2008).

Further, in VWM task the strength of α- and β-band synchronization in the PPC correlated with individual VWM capacity limits, while the attentional capacity in this study was correlated with the strength of synchronization between visual and frontal cortices as well as within visual system bilaterally. As in the VWM, also in visual attention, the strength of CFC interactions was correlated with individual attentional capacity albeit with slightly different spectral patterns (Siebenhühner et al. 2016). These results point to important similarities but also differences in how synchronization may connect functionally relevant brain regions in visual attention and VWM.

Our results complement prior studies showing that both local γ oscillations in source-reconstructed MEG data (Palva et al. 2011; Rouhinen et al. 2013) as well as slow contralateral delay activity in scalp EEG recordings (Vogel and Machizawa 2004; Vogel et al. 2005; Drew and Vogel 2008; Drew et al. 2011, 2012) correlate both with the number of items held in VWM as well as in the focus of attention in MOT tasks. Taken together, these evidence support the hypothesis that attended perception and VWM have partially shared underlying neuronal mechanism based on processing related to multiband oscillations across fronto-parietal and sensory brain regions (Watrous et al. 2015a, 2015b).

Conclusions

Our study shows that individual attentional capacity is positively correlated with load-dependent strengthening of large-scale synchronization and CFC. Our findings support the

framework where lα synchronization coordinates attentional processing (Palva and Palva 2007, 2011) by providing "frames" for sensory processing (Lakatos et al. 2008; Schroeder et al. 2010; VanRullen 2016; Palva and Palva 2018), while the γ-band synchronization contributes to the processing of visual stimulus information (Bosman et al. 2012; Siegel et al. 2012). Our observations are also consistent with CFC among these oscillations underlying the integration of these functions (Palva et al. 2005; Palva and Palva 2007, 2017, 2018; Schroeder and Lakatos 2009a; Lisman and Jensen 2013).

Supplementary Data

Supplementary material is available at *Cerebral Cortex* online.

Funding

References

Alnaes D, Sneve MH, Richard G, Skatun KC, Kaufmann T, Nordvik JE, Andreassen OA, Endestad T, Laeng B, Westlye LT. 2015. Functional connectivity indicates differential roles for the intraparietal sulcus and the superior parietal lobule in multiple object tracking. *Neuroimage*. 123: 129–137.

Alvarez GA, Cavanagh P. 2005. Independent resources for attentional tracking in the left and right visual hemifields. *Psychol Sci*. 16:637–643.

Axmacher N, Henseler MM, Jensen O, Weinreich I, Elger CE, Fell J. 2010. Cross-frequency coupling supports multi-item working memory in the human hippocampus. *Proc Natl Acad Sci USA*. 107:3228–3233.

Bahramisharif A, Jensen O, Jacobs J, Lisman J. 2018. Serial representation of items during working memory maintenance at letter-selective cortical sites. *PLoS Biol*. 16:e2003805.

Battelli L, Cavanagh P, Intriligator J, Tramo MJ, Henaff MA, Michel F, Barton JJ. 2001. Unilateral right parietal damage leads to bilateral deficit for high-level motion. *Neuron*. 32: 985–995.

Bettencourt KC, Somers DC. 2009. Effects of target enhancement and distractor suppression on multiple object tracking capacity. *J Vis*. 9:9.

Bettencourt KC, Michalka SW, Somers DC. 2011. Shared filtering processes link attentional and visual short-term memory capacity limits. *J Vis*. 11. doi: 10.1167/11.10.22.

Bosman CA, Schoffelen JM, Brunet N, Oostenveld R, Bastos AM, Womelsdorf T, Rubehn B, Stieglitz T, De Weerd P, Fries P. 2012. Attentional stimulus selection through selective synchronization between monkey visual areas. *Neuron*. 75: 875–888.

Brunton BW, Beyeler M. 2019. Data-driven models in human neuroscience and neuroengineering. *Curr Opin Neurobiol*. 58:21–29.

Bullmore E, Sporns O. 2009. Complex brain networks: graph theoretical analysis of structural and functional systems. *Nat Rev Neurosci*. 10:186–198.

Canolty RT, Knight RT. 2010. The functional role of cross-frequency coupling. *Trends Cogn Sci*. 14:506–515.

Corbetta M, Shulman GL. 2002. Control of goal-directed and stimulus-driven attention in the brain. *Nat Rev Neurosci.* 3:201–215.

Visconti PE, Muschietti JP, Flawia MM, Tezon JG. 1990. Bicarbonate dependence of cAMP accumulation induced by phorbol esteres in hamster spermatozoa. *Biochem Biophys Acta.* 1054:231–6.

Cowan N, Elliott EM, Scott Saults J, Morey CC, Mattox S, Hismjatullina A, Conway AR. 2005. On the capacity of attention: its estimation and its role in working memory and cognitive aptitudes. *Cogn Psychol.* 51:42–100.

Culham JC, Brandt SA, Cavanagh P, Kanwisher NG, Dale AM, Tootell RB. 1998. Cortical fMRI activation produced by attentive tracking of moving targets. *J Neurophysiol.* 80: 2657–2670.

Daitch AL, Sharma M, Roland JL, Astafiev SV, Bundy DT, Gaona CM, Snyder AZ, Shulman GL, Leuthardt EC, Corbetta M. 2013. Frequency-specific mechanism links human brain networks for spatial attention. *Proc Natl Acad Sci USA.* 110:19585–19590.

Dale AM, Liu AK, Fischl BR, Buckner RL, Belliveau JW, Lewine JD, Halgren E. 2000. Dynamic statistical parametric mapping: combining fMRI and MEG for high-resolution imaging of cortical activity. *Neuron.* 26:55–67.

D'Andrea A, Chella F, Marshall TR, Pizzella V, Romani GL, Jensen O, Marzetti L. 2019. Alpha and alpha-beta phase synchronization mediate the recruitment of the visuospatial attention network through the superior longitudinal fasciculus. *Neuroimage.* 188:722–732.

Destrieux C, Fischl B, Dale A, Halgren E. 2010. Automatic parcellation of human cortical gyri and sulci using standard anatomical nomenclature. *Neuroimage.* 53:1–15.

Doesburg SM, Bedo N, Ward LM. 2016. Top-down alpha oscillatory network interactions during visuospatial attention orienting. *Neuroimage.* 132:512–519.

Drew T, Vogel EK. 2008. Neural measures of individual differences in selecting and tracking multiple moving objects. *J Neurosci.* 28:4183–4191.

Drew T, Horowitz TS, Wolfe JM, Vogel EK. 2011. Neural measures of dynamic changes in attentive tracking load. *J Cogn Neurosci.* 24:440–450.

Drew T, Horowitz TS, Vogel EK. 2012. Swapping or dropping? Electrophysiological measures of difficulty during multiple object tracking. *Cognition.* 126:213–223.

Fell J, Axmacher N. 2011. The role of phase synchronization in memory processes. *Nat Rev Neurosci.* 12:105–118.

Fischl B, van der Kouwe A, Destrieux C, Halgren E, Segonne F, Salat DH, Busa E, Seidman LJ, Goldstein J, Kennedy D, et al. 2004. Automatically parcellating the human cerebral cortex. *Cereb Cortex.* 14:11–22.

Fries P. 2015. Rhythms for cognition: communication through coherence. *Neuron.* 88:220–235.

Gaspar JM, Christie GJ, Prime DJ, Jolicoeur P, McDonald JJ. 2016. Inability to suppress salient distractors predicts low visual working memory capacity. *Proc Natl Acad Sci USA.* 113:3693–3698.

Glennon M, Keane MA, Elliott MA, Sauseng P. 2016. Distributed cortical phase synchronization in the EEG reveals parallel attention and working memory processes involved in the attentional blink. *Cereb Cortex.* 26:2035–2045.

Gramfort A, Luessi M, Larson E, Engemann DA, Strohmeier D, Brodbeck C, Parkkonen L, Hämäläinen MS. 2014. MNE software for processing MEG and EEG data. *Neuroimage.* 86:446–460.

Grill-Spector K, Malach R. 2004. The human visual cortex. *Annu Rev Neurosci.* 27:649–677.

Gross J, Schmitz F, Schnitzler I, Kessler K, Shapiro K, Hommel B, Schnitzler A. 2004. Modulation of long-range neural synchrony reflects temporal limitations of visual attention in humans. *Proc Natl Acad Sci USA.* 101:13050–13055.

Harding IH, Yucel M, Harrison BJ, Pantelis C, Breakspear M. 2015. Effective connectivity within the frontoparietal control network differentiates cognitive control and working memory. *Neuroimage.* 106:144–153.

Harper J, Malone SM, Iacono WG. 2017. Theta- and delta-band EEG network dynamics during a novelty oddball task. *Psychophysiology.* 54:1590–1605.

Herring JD, Thut G, Jensen O, Bergmann TO. 2015. Attention modulates TMS-locked alpha oscillations in the visual cortex. *J Neurosci.* 35:14435–14447.

Hillebrand A, Barnes GR. 2002. A quantitative assessment of the sensitivity of whole-head MEG to activity in the adult human cortex. *Neuroimage.* 16:638–650.

Howe PD, Horowitz TS, Morocz IA, Wolfe J, Livingstone MS. 2009. Using fMRI to distinguish components of the multiple object tracking task. *J Vis.* 9:10.1–10.11.

JASP Team 2016. JASP (version 0.8.0) [computer software] https://jasp-stats.org/.

Jensen O, Mazaheri A. 2010. Shaping functional architecture by oscillatory alpha activity: gating by inhibition. *Front Hum Neurosci.* 4:186.

Jensen O, Gips B, Bergmann TO, Bonnefond M. 2014. Temporal coding organized by coupled alpha and gamma oscillations prioritize visual processing. *Trends Neurosci.* 37:357–369.

Jensen O, Colgin LL. 2007. Cross-frequency coupling between neuronal oscillations. *Trends in Cognitive Sciences.* 11: 267–269.

Jovicich J, Peters RJ, Koch C, Braun J, Chang L, Ernst T. 2001. Brain areas specific for attentional load in a motion-tracking task. *J Cogn Neurosci.* 13:1048–1058.

Kastner S, Ungerleider LG. 2000. Mechanisms of visual attention in the human cortex. *Annu Rev Neurosci.* 23:315–341.

Klimesch W, Freunberger R, Sauseng P, Gruber W. 2008. A short review of slow phase synchronization and memory: evidence for control processes in different memory systems? *Brain Res.* 1235:31–44.

Korhonen O, Palva S, Palva JM. 2014. Sparse weightings for collapsing inverse solutions to cortical parcellations optimize M/EEG source reconstruction accuracy. *J Neurosci Methods.* 226C:147–160.

Kreiter AK, Singer W. 1996. Stimulus-dependent synchronization of neuronal responses in the visual cortex of the awake macaque monkey. *J Neurosci.* 16:2381–2396.

Lahnakoski JM, Jaaskelainen IP, Sams M, Nummenmaa L. 2017. Neural mechanisms for integrating consecutive and interleaved natural events. *Hum Brain Mapp.* 38:3360–3376.

Lakatos P, Karmos G, Mehta AD, Ulbert I, Schroeder CE. 2008. Entrainment of neuronal oscillations as a mechanism of attentional selection. *Science.* 320:110–113.

Lakatos P, Gross J, Thut G. 2019. A new unifying account of the roles of neuronal entrainment. *Curr Biol.* 29:R890–R905.

Lapierre MD, Cropper SJ, Howe PDL. 2017. Shared processing in multiple object tracking and visual working memory in the absence of response order and task order confounds. *PLoS One.* 12:e0175736.

Lisman JE, Jensen O. 2013. The theta-gamma neural code. *Neuron.* 77:1002–1016.

Lobier M, Palva JM, Palva S. 2017. High-alpha band synchronization across frontal, parietal and visual cortex mediates behavioral and neuronal effects of visuospatial attention. *Neuroimage*. 165:222–237.

Lozano-Soldevilla D, Ter Huurne N, Oostenveld R. 2016. Neuronal oscillations with non-sinusoidal morphology produce spurious phase-to-amplitude coupling and directionality. *Front Comput Neurosci*. 10:87.

Luck SJ, Vogel EK. 1997. The capacity of visual working memory for features and conjunctions. *Nature*. 390:279–281.

Mäki-Marttunen V, Hagen T, Laeng B, Espeseth T. 2020. Distinct neural mechanisms meet challenges in dynamic visual attention due to either load or object spacing. *J Cogn Neurosci*. 32:65–84.

Meehan TP, Bressler SL, Tang W, Astafiev SV, Sylvester CM, Shulman GL, Corbetta M. 2017. Top-down cortical interactions in visuospatial attention. *Brain Struct Funct*. 222: 3127–3145.

Nolte G, Bai O, Wheaton L, Mari Z, Vorbach S, Hallett M. 2004. Identifying true brain interaction from EEG data using the imaginary part of coherency. *Clin Neurophysiol*. 115:2292–2307.

Oksama L, Hyona J. 2004. Is multiple object tracking carried out automatically by an early vision mechanism independent of higher-order cognition? An individual difference approach. *Visual Cognition*. 11:631–671.

Oostenveld R, Fries P, Maris E, Schoffelen JM. 2011. FieldTrip: open source software for advanced analysis of MEG, EEG, and invasive electrophysiological data. *Comput Intell Neurosci*. 2011:156869.

Palva JM, Palva S. 2017. Functional integration across oscillation frequencies by cross-frequency phase synchronization. *Eur J Neurosci*. 48:2399–2406.

Palva S, Palva JM. 2018. Roles of brain criticality and multi-scale oscillations in sensorimotor predictions. *Trends Neurosci*. 41:729–743.

Palva JM, Palva S, Kaila K. 2005. Phase synchrony among neuronal oscillations in the human cortex. *J Neurosci*. 25:3962–3972.

Palva JM, Monto S, Kulashekhar S, Palva S. 2010. Neuronal synchrony reveals working memory networks and predicts individual memory capacity. *Proc Natl Acad Sci USA*. 107:7580–7585.

Palva JM, Wang SH, Palva S, Zhigalov A, Monto S, Brookes MJ, Schoffelen J, Jerbi K. 2018. Ghost interactions in MEG/EEG source space: a note of caution on inter-areal coupling measures. *NeuroImage*. 173:632–643.

Palva S, Palva JM. 2007. New vistas for alpha-frequency band oscillations. *Trends Neurosci*. 30:150–158.

Palva S, Kulashekhar S, Hamalainen M, Palva JM. 2011. Localization of cortical phase and amplitude dynamics during visual working memory encoding and retention. *J Neurosci*. 31:5013–5025.

Palva S, Palva JM. 2011. Functional roles of alpha-band phase synchronization in local and large-scale cortical networks. *Front Psychol*. 2:204.

Palva S, Palva JM. 2012. Discovering oscillatory interaction networks with M/EEG: challenges and breakthroughs. *Trends Cogn Sci*. 16:219–230.

Ptak R. 2012. The frontoparietal attention network of the human brain: action, saliency, and a priority map of the environment. *Neuroscientist*. 18:502–515.

Pylyshyn ZW, Storm RW. 1988. Tracking multiple independent targets: evidence for a parallel tracking mechanism. *Spat Vis*. 3:179–197.

Riesenhuber M, Poggio T. 2002. Neural mechanisms of object recognition. *Curr Opin Neurobiol*. 12:162–168.

Robitaille N, Marois R, Todd J, Grimault S, Cheyne D, Jolicoeur P. 2010. Distinguishing between lateralized and nonlateralized brain activity associated with visual short-term memory: FMRI, MEG, and EEG evidence from the same observers. *Neuroimage*. 53:1334–1345.

Rouhinen S, Panula J, Palva JM, Palva S. 2013. Load dependence of beta and gamma oscillations predicts individual capacity of visual attention. *J Neurosci*. 33:19023–19033.

Sadaghiani S, Hesselmann G, Kleinschmidt A. 2009. Distributed and antagonistic contributions of ongoing activity fluctuations to auditory stimulus detection. *J Neurosci*. 29:13410–13417.

Sauseng P, Klimesch W, Heise KF, Gruber WR, Holz E, Karim AA, Glennon M, Gerloff C, Birbaumer N, Hummel FC. 2009. Brain oscillatory substrates of visual short-term memory capacity. *Curr Biol*. 19:1846–1852.

Sayres R, Grill-Spector K. 2008. Relating retinotopic and object-selective responses in human lateral occipital cortex. *J Neurophysiol*. 100:249–267.

Schroeder CE, Lakatos P. 2009a. The gamma oscillation: master or slave? *Brain Topogr*. 22:24–26.

Schroeder CE, Lakatos P. 2009b. Low-frequency neuronal oscillations as instruments of sensory selection. *Trends Neurosci*. 32:9–18.

Schroeder CE, Wilson DA, Radman T, Scharfman H, Lakatos P. 2010. Dynamics of active sensing and perceptual selection. *Curr Opin Neurobiol*. 20:172–176.

Siebenhühner F, Wang SH, Palva JM, Palva S. 2016. Cross-frequency synchronization connects networks of fast and slow oscillations during visual working memory maintenance. *Elife*. 5:e13451.

Siebenhühner F, Wang SH, Arnulfo G, Lampinen A, Nobili L, Palva JM, Palva S. Forthcoming 2020. Genuine cross-frequency coupling networks in human resting-state electrophysiological recordings. *PLOS Biol*. 18:e3000685. https://doi.org/10.1371/journal.pbio.3000685.

Siegel M, Donner TH, Oostenveld R, Fries P, Engel AK. 2008. Neuronal synchronization along the dorsal visual pathway reflects the focus of spatial attention. *Neuron*. 60: 709–719.

Siegel M, Donner TH, Engel AK. 2012. Spectral fingerprints of large-scale neuronal interactions. *Nat Rev Neurosci*. 13:121–134.

Singer W. 2009. Distributed processing and temporal codes in neuronal networks. *Cogn Neurodyn*. 3:189–196.

Spadone S, Della Penna S, Sestieri C, Betti V, Tosoni A, Perrucci MG, Romani GL, Corbetta M. 2015. Dynamic reorganization of human resting-state networks during visuospatial attention. *Proc Natl Acad Sci USA*. 112:8112–8117.

Tass P, Rosenblum MG, Weule J, Kurths J, Pikovsky A, Volkmann J, Schnitzler A, Freund HJ. 1998. Detection of n:M phase locking from noisy data: application to magnetoencephalography. *Phys Rev Lett*. 81:3291–3294.

Todd JJ, Marois R. 2004. Capacity limit of visual short-term memory in human posterior parietal cortex. *Nature*. 428:751–754.

Treisman A. 2006. How the deployment of attention determines what we see. *Vis Cogn*. 14:411–443.

VanRullen R. 2016. Perceptual cycles. *Trends Cogn Sci*. 20:723–735.

Vinberg J, Grill-Spector K. 2008. Representation of shapes, edges, and surfaces across multiple cues in the human visual cortex. *J Neurophysiol*. 99:1380–1393.

Vinck M, Oostenveld R, van Wingerden M, Battaglia F, Pennartz CM. 2011. An improved index of phase-synchronization for electrophysiological data in the presence of volume-conduction, noise and sample-size bias. *Neuroimage*. 55:1548–1565.

Vogel EK, Machizawa MG. 2004. Neural activity predicts individual differences in visual working memory capacity. *Nature*. 428:748–751.

Vogel EK, McCollough AW, Machizawa MG. 2005. Neural measures reveal individual differences in controlling access to working memory. *Nature*. 438:500–503.

Voytek B, Canolty RT, Shestyuk A, Crone NE, Parvizi J, Knight RT. 2010. Shifts in gamma phase-amplitude coupling frequency from theta to alpha over posterior cortex during visual tasks. *Front Hum Neurosci*. 4:191.

Wang S, Lobier L, Siebenhühner F, Puoliväli T, Palva S, Palva J. 2018. Hyperedge bundling: a practical solution to spurious interactions in MEG/EEG connectivity analyses. *NeuroImage*. 173:610–622.

Watrous AJ, Deuker L, Fell J, Axmacher N. 2015a. Phase-amplitude coupling supports phase coding in human ECoG. *Elife*. 24;4.

Watrous AJ, Fell J, Ekstrom AD, Axmacher N. 2015b. More than spikes: common oscillatory mechanisms for content specific neural representations during perception and memory. *Curr Opin Neurobiol*. 31:33–39.

Westfall PH, Johnson WO, Utts JM. 1997. A bayesian perspective on the bonferroni adjustment. *Biomet*. 84:419–427.

Womelsdorf T, Everling S. 2015. Long-range attention networks: circuit motifs underlying endogenously controlled stimulus selection. *Trends Neurosci*. 38:682–700.

Womelsdorf T, Lima B, Vinck M, Oostenveld R, Singer W, Neuenschwander S, Fries P. 2012. Orientation selectivity and noise correlation in awake monkey area V1 are modulated by the gamma cycle. *Proc Natl Acad Sci USA*. 109:4302–4307.

Xu Y, Chun MM. 2006. Dissociable neural mechanisms supporting visual short-term memory for objects. *Nature*. 440:91–95.

Yeo BT, Krienen FM, Sepulcre J, Sabuncu MR, Lashkari D, Hollinshead M, Roffman JL, Smoller JW, Zollei L, Polimeni JR, et al. 2011. The organization of the human cerebral cortex estimated by intrinsic functional connectivity. *J Neurophysiol*. 106:1125–1165.

Zhou H, Desimone R. 2011. Feature-based attention in the frontal eye field and area V4 during visual search. *Neuron*. 70:1205–1217.